RSC Advances

ROYAL SOCIETY OF CHEMISTRY

www.rsc.org/advances

Electrical and magnetic properties of the pulsed laser deposited Ca doped $LaMnO_3$ thin films on Si (100) and their electronic structures

Khalid Sultan[1*,] M. Ikram*[1] Sanjeev Gautam[2,3], Han -Koo Lee[4], KeunHwa Chae[2], and K.Asokan[5]

[1]Solid State Physics Lab. Department of Physics, National Institute of Technology Hazratbal Srinagar, J & K-190006, India
[2]Advanced Analysis Center, Korea Institute of Science and Technology (KIST), Seoul 136-791, South Korea
[3]Dr. S.S. Bhatnagar University Institute of Chemical Engineering and Technology (SSB UICET), Panjab University Chandigarh, 160-014, India
[4]Beamline Research Division, Pohang Accelerator Lab (POSTECH), Pohang 790-834, South Korea
[5]Materials Science Division, Inter University Accelerator Centre, New Delhi-110067, India

Abstract

We report the effect of Ca doping on the structural, electrical, magnetic and electronic properties of stoichiometric $La_{1-x}Ca_xMnO_3$ (x=0, 0.3, 0.5 and 0.7) (LCMO) thin films grown on Si (100) by pulsed laser deposition technique. All these films exhibit a single-phase orthorhombic structure with space group *Pnma*. The physical properties like surface roughness, grains size, Curie temperature 'Tc', activation energy 'Ea' and magneto-resistance were studied as a function of Ca doping. These properties were correlated with the variation of the observed electrical transport and magnetic properties and their electronic structures. Electronic structures of these films were studied by X-ray absorption spectroscopy (XAS) at O K-, and Mn $L_{3,2}$-edges and indicate admixture of Mn^{2+}, Mn 3^+, and Mn^{4+}ions and also increase in density of states with Ca doping. This mixed valence states of Mn ions in LCMO arise due to the doping of Ca in the La sites and modify the electrical and magnetic properties.

Key Words: PLD, XAS, GIXRD, Magnetization.
*Corresponding author Tel.: +91 -8717000375
*Email:ksbhat.phy@gmail.com; ikram@nitsri.net

1. Introduction

Even after five decades of research, doping studies of divalent cations like Ca ion in manganites fascinates because of the evolution of complex phase diagram comprising of a rich variety of crystallographic, magnetic, and electronic phases [1-3]. It also exhibits the strong interplay between the spin, charge, orbital, and lattice degrees of freedom. All these are dependent on the doping concentration. These doping studies show drastic changes in the magnetic and transport properties even by subtle modifications in the chemical composition and external parameters like temperature, pressure etc[4]. $LaMnO_3$ was found to have an orthorhombic structure with space group *Pnma.* The deviation of structure from cubic is usually attributed to the Jahn-Teller instability of the Mn^{3+} ions. On the other hand, $CaMnO_3$ is thought to have a structure closer to cubic than to $LaMnO_3$(LMO) as the Mn^{4+} ions does not produce any Jahn-Teller distortion [5].The valency of Mn ions (Mn^{3+}/Mn^{4+}), oxygen stoichiometry and the ratio between trivalent and divalent cations (R^{3+}/A^{2+}) determines the magnetic and electrical properties in the compound [5]. The observed behavior in these compounds is explained on the basis of double exchange mechanism [6-8], Jahn-Teller distortion [9], lattice, charge and orbital degrees of freedom and as well as phase separation [10-12].The strong correlation between the observed transport and magnetic properties results in novel phenomena with possible future applications.

Magneto-electronic devices are often fabricated in the form of thin films. These applications require films of high quality, homogeneous and smooth surface morphology. Many novel techniques have been employed to synthesize LMO thin films such as sol–gel, Atomic layer deposition (ALD), molecular beam epitaxy (MBE), spray pyrolysis, etc [13-17]. Several studies focused on pulsed Laser deposition (PLD) deposited thin films of Ca doped LMO [18]. PLD is a

well-established technique for depositing high-quality thin films even with a complex stoichiometry. Due to the high energy of the laser and the short pulse duration (~25 ns) the laser-target material interaction is predominantly photonic with only a minimum thermal heating. Moreover, when the material is fabricated as thin film, the crystal structure and chemical composition at the surface can have a significant influence.

Commonly, $SrTiO_3$ (STO) and $LaAlO_3$ (LAO) single crystals, having the lattice constants a_{STO}= 3.91 and a_{LAO}= 3.79 Å, respectively, are used as substrates because of their lattice match to that of bulk LMO. Theoretically, this allows the growth of single crystalline, and epitaxial films. On the other hand, thin films on Si a_{Si}= 5.43 Å are expected to have large lattice mismatch and results in polycrystalline. Hence depositing LMO films on Si adds strain due to the large lattice mismatch and surface roughness. It is also well known that the surface composition of rare-earth manganites differs from bulk, due to segregation effects [19, 20]. In the case of LMO, the formal valencies are La^{3+} Mn^{3+} $O^{2-}{}_3$ and for $CaMnO_3$, $Ca^{2+}Mn^{4+}O^{2-}{}_3$, so that (La, Ca) MnO_3 should contain both Mn^{3+} and Mn^{4+} ions. This mixed valency nature modifies the magnetic and electronic properties of the system. For instance, parent compounds $LaMnO_3$ and $CaMnO_3$ are antiferromagnetic insulators at low temperature but $La_{0.7}Ca_{0.3}MnO_3$(LCMO) is a ferromagnetic metal. The mixed valence states of Mn ions modify the electrical and magnetic properties of the LCMO system. To understand local electronic structure including the valence of Mn, and hybridization of Mn 3d-O 2p states, X-ray absorption spectroscopy (XAS) is an excellent technique. It has been used extensively in transition metal oxides.

Present study focuses on the structure, morphology, transport, magnetic and magnetoresistance properties of the LCMO films fabricated on Si substrates and their modifications in their electronic structures. The emphasis is to understand these physical

properties and electronic structures to correlate with the phase diagram of Ca doped $LaMnO_3$ thin films fabricated on Si substrates

2. Experimental details:

Targets of compositions of $La_{1-x}Ca_xMnO_3$ (x=0.0, 0.3, 0.5 and 0.7) (hereafter referred as LCMO) were prepared using a conventional solid state reaction technique. Mixed powders of La_2O_3, Mn_2O_3 and $CaCO_3$ taken in the stoichiometry ratio were preheated at 1000^{o}C for 12 hours and calcinated again at 1200^{o}C for 12 hours and sintered. Thin films of LCMO on Si (100) were prepared by the PLD method. The chamber was cleaned prior to PLD deposition and the base pressure was maintained at ~1×10^{-5}Torr. A Lambda-Physik LPX210 krypton-fluorine excimer laser (wavelength 248 nm, pulse length 20 ns, repetition rate10 Hz) was used to deliver a pulsed-laser beam of energy density 1.8 J cm^{-2} at the target surface. The target-substrate distance was kept 5 cm. The substrate was kept at 750^{o}C during the deposition to ensure highly oriented growth. The ablation was carried out in oxygen at a partial pressure of 330 mTorr. The deposition was carried out for 17 minutes with laser energy of 200 mJ. After deposition, the films were cooled down to room temperature in the ambient oxygen pressure at 20^{o}C /min. The film thickness was estimated around 70 ± 5 nm using XP1 Tely step profilometer.

The films were characterized by X-ray diffraction (XRD) Bruker AXS D8 Discover (Cu-Kα radiation) at room temperature in the 2θ range of 20-80^o. Surface morphology was studied using atomic force microscope (AFM) Nanoscope E-digital instrument. Inc USA in contact mode. The magnetic measurements were carried out using a 7-Tesla MPMS SQUID-VSM. The temperature dependent magnetization was carried out from 5K to 300K at a field of 100 Oe both in Field cooled (FC) as well as in Zero field cooled (ZFC) condition. Electrical resistances R (H)

under a magnetic field H was measured from 5 K to 300 K by using standard four-probe technique. All these electrical and magnetic measurements were carried out at IUC, CSR Indore.

The X-ray absorption spectra at O K-, and Mn $L_{3,2}$ edges were performed at the soft X-ray beamline 10D XAS KIST (Korea Institute of Science and Technology) of the Pohang light source (PLS), (S. Korea) operating at 2.5 GeV with a constant (top-up mode) storage current of 400 mA. The spectra were measured using the sample drain current mode (TEY) at room temperature and the vacuum in the experimental chamber was in the low range of 10^{-9}Torr. The resolution of the spectra was better than 0.6 eV at O K-edge. The data is normalized to the edge-jump at post-edge region after removing the background at pre-edge straight region.

3. Results and discussions

3.1 Structural and morphological studies

Fig. 1 shows the glancing incidence XRD (GIXRD) pattern of LCMO thin films. All these films were of polycrystalline without detectable secondary phases and indexed with the orthorhombic structure of space group *Pnma*. Abrashev *et al* [21] reported that unlike other perovskite manganites, the average crystal structure of $La_{1-x}Ca_xMnO_3$ remains orthorhombic in the entire range of Ca substitution at temperature below ~700 K. With neutron and X-ray diffraction, Rodriguez *et al* [22] confirmed that $LaMnO_3$ has an orthorhombic structure below ~800 K. The compositions with x= 0.5 and x = 0.83 can be indexed with the pseudocubic perovskite structure at room temperature and cubic to tetragonal structural phase transition arises on lowering the temperature as reported by Zheng*et al* [23]. It has been reported by Banerjee and Krishnan [24] that $LaMnO_3$ crystallizes in rhombohedral structure (R 3–c) with a small distortion. Nagabbushane *et al* [25] reported that that nano crystalline $LaMnO_3$ synthesized by combustion process are in cubic phase.

On calcinations at 900 °C, the structure of Ca doped manganites changes to rhombohedral phase while pristine $LaMnO_3$ retained the cubic phase. All these studies show that the crystal structure of $LaMnO_3$ is highly sensitive to preparation conditions and the physical properties are highly dependent on the structure.

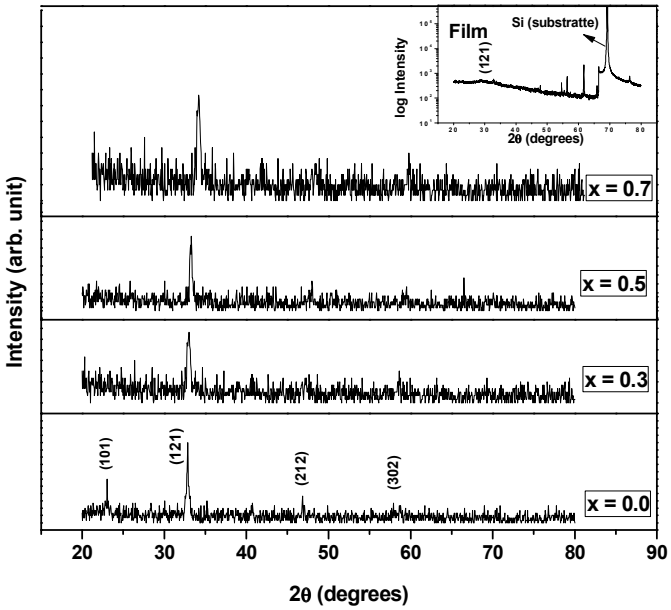

Fig.1. The GIXRD pattern of LCMO thin films. Inset shows the XRD pattern with substrate.

Further, the strain, (ε), was calculated using Williamson Hall equations: $\beta = \frac{K\lambda}{D cos\theta} + 4\varepsilon\, tan\theta$. Rearranging this equation, one gets

$$\beta cos\theta = \frac{K\lambda}{D} + 4\varepsilon\, sin\theta$$

By linear extrapolation of the plot, βcosθ *vs* 4sinθ along *y* and *x* axis respectively, the crystallite size is obtained at the intercept of Kλ/D and the strain (ε) from the slope. In this, β and θ are taken in radians.

Table-I.

The lattice parameters of LCMO films deposited on Si (100) substrates.

Film	**a (Å)**	**b (Å)**	**c (Å)**	**FWHM (degrees)**	**Strain (x 10^{-1})**
x = 0	5.521	7.712	5.541	0.416	1.07
x = 0.3	5.413	7.733	5.489	0.431	1.11
x = 0.5	5.425	7.669	5.431	0.425	1.09
x = 0.7	5.312	7.570	5.391	0.496	1.20

The lattice parameters, full width half maximum (FWHM) calculated from peak (121) and strain are tabulated in Table I. With Ca doping, it is observed that the calculated strain and FWHM increases but the intensity decreases marginally indicating change in the crystallinity of the LCMO thin films. In addition, there was deviation in lattice parameters.

The cations, La and Ca, have almost similar ionic radii and are randomly substituted on A site. The size of the ions determines the extent of distortion in the compound. If the size of A site cation $r_A < a/\sqrt{2}-r_o$ (here 'a' is the cubic lattice parameter and r_o is the radius of oxygen ion), the distortion will be most probably due to rigid tilts of oxygen octahedra. On contrary if $r_B < a/2-r_o$ ($r_{B\ is}$ the radius of B site cation) the distortion is most likely due to movement of B site cation within the oxygen octahedra. Present study follows the former ($r_A < a/\sqrt{2}-r_o$) relation between its

contributing ions and probably distorted by rotation of oxygen octahedral at room temperature. This variation has been attributed to the decrease in effective ionic radii of La and Mn on Ca doping. The distortion of MnO_6 octahedra depends not only on the ionic radii of dopants but also on the amount of doping.

Fig.2 shows the AFM images of LCMO thin films. The surface roughness of these films is in the range of 1.86 nm, 2.64 nm, 2.27 nm and 2.62 nm respectively for x=0,0.3, 0.5 and 0.7. The values listed in Table II suggest that films are extremely smooth in general. There are very small grains with an average diameter of about 44 nm, 46 nm, 45 nm and 51 nm respectively for x = 0.0, 0.3, 0.5 and 0.7. The observed grain diameters of these films prepared by PLD were less compared to those prepared by other groups [17] using ALD technique. This implies the role of deposition techniques on grain formation. This study shows that with Ca doping, there is change in surface roughness and grain sizes of the LCMO films.

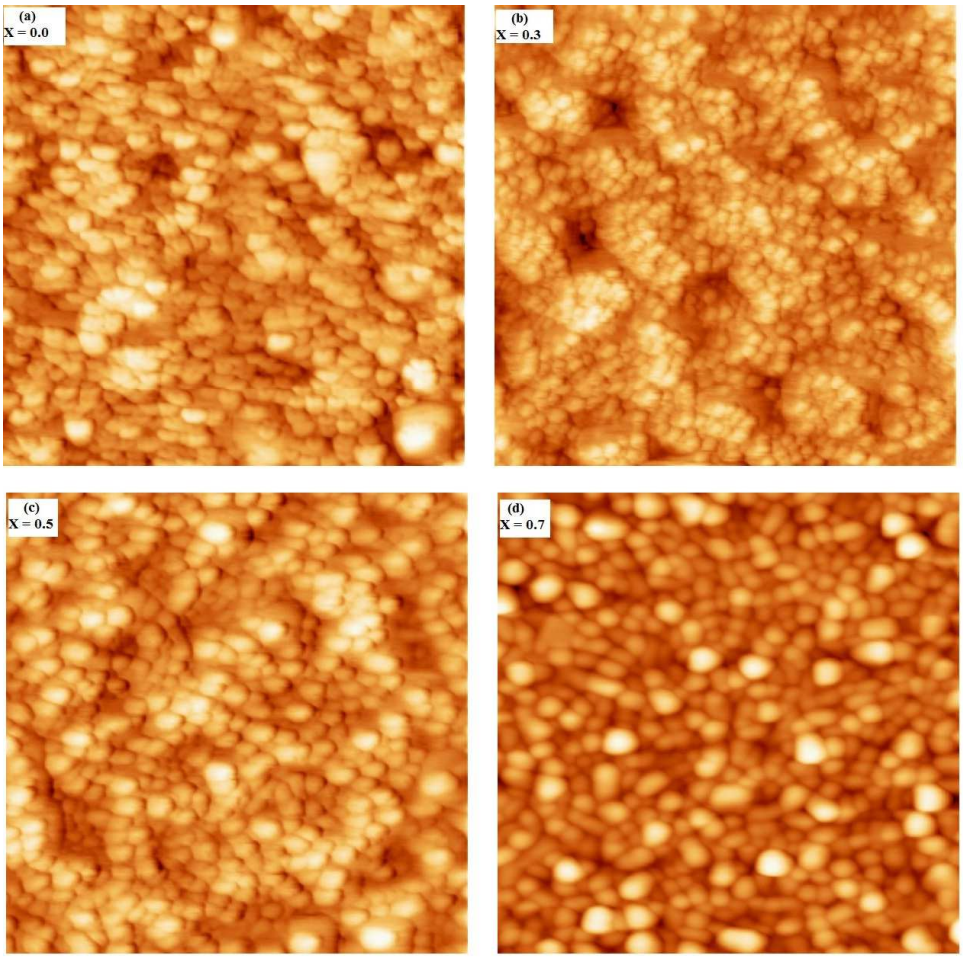

Fig.2. AFM images (size,1 μm x 1 μm) of LCMO films on Si (100): (a) x = 0.0, (b) x= 0.3, (c) x= 0.5, and (d) x= 0.7.

3.2 Magnetic measurements

The ZFC and field-cooled FC magnetization as a function of temperature at 100 Oe field are shown in figure 3. The large difference between FC and ZFC curves at low temperatures suggests an inhomogeneous mixture of a ferromagnetic and anti-ferromagnetic ordering rather than a distinct long range order. This also indicates the presence of magnetic ordering in the film. Appearance of peaks in the ZFC curves is the characteristic of blocking mechanism owing to the competition between the thermal energy and the magnetic anisotropy energy of particles. The magnetic transition temperature 'Tc' (the temperature at which the maximum slope dM/dT

occurs), for x = 0.0, 0.3 and 0.5 are 140 K, 230 K and 235 K for respectively. The values of ferromagnetic curie temperature (Tc), blocking temperature (T_B), saturation magnetization (Ms), retentivity (Mr) and coercivity (Hc) for the LCMO films are tabulated in Table II. It is observed that the value of Tc increases with Ca doping in the LCMO system up to x = 0.5. For the composition x = 0.7, no sharp magnetic transition is observed. The calculated magnetic parameters Ms, Mr and Hc show an increase with Ca doping indicating the magnetic ordering in films with Ca doping. No anomaly was observed in MT spectra of LMO as observed by Khanduri*et al* [14], where it has been reported that LMO shows broad anomalies at 44 K and 211 K in magnetization vs. Temperature curve. Absence of such anomalies may be attributed to a different preparation technique (PLD) and possibly due to different calcination temperature used in this study during the preparation of films. The shift in transition temperature "Tc" of different doping concentrations may arise due to the presence of lattice disorder and/or strain in the films. The value of magnetic moment increases progressively with Ca doping but decreases for higher doping (x = 0.7). Magnetization (M) both FC and ZFC increase rapidly below Tc. At lower temperatures the M becomes saturated in FC case due to the fully ordered Mn^{3+} and Mn^{4+} pairs. However, in case of ZFC magnetization, M does not become saturated even at lower temperatures.

In LCMO, there are three basic phases: insulating-paramagnetic, ferromagnetic, with metallic-like conductivity and charge-ordered antiferromagnetic insulating phases. The parent compound, LMO is an antiferromagnetic insulator and the Ca doping at La sites results in the phenomenon of colossal magneto-resistance (CMR) for the doping range of $0.2 < x < 0.5$. The phenomena of CMR occur in these compositions as a consequence of rapid shift of

ferromagnetic transition temperature (Tc) to higher temperature region in the presence of magnetic field.

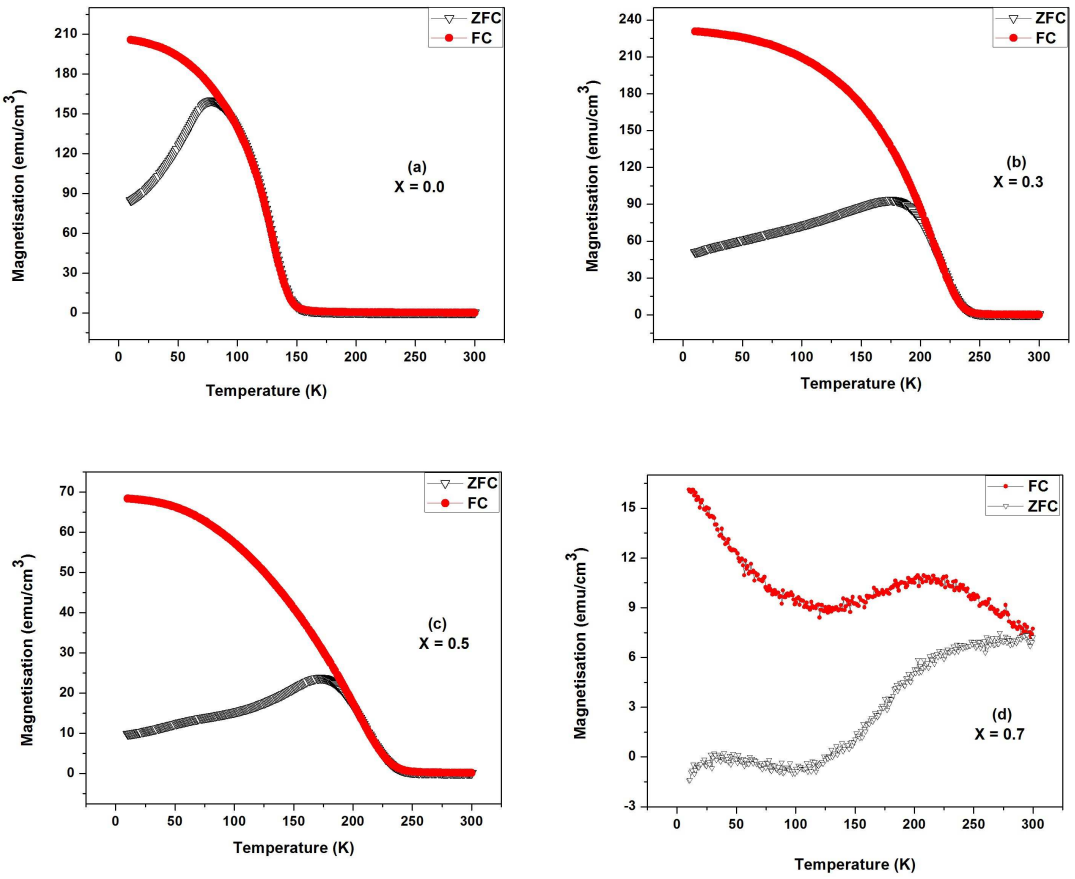

Fig.3. Temperature dependence of ZFC and FC magnetization plots (in the presence of 100 Oe magnetic field) LCMO films for (a) x= 0.0, (b)x = 0.3, (c) x= 0.5, and (d) x = 0.7. It is observed that the value of Tc increases with Ca doping in the LCMO system up to x = 0.5. For the composition x = 0.7, there is no sharp magnetic transition.

Table-II. The values of various calculated parameters such as grain diameter, surface roughness, ferromagnetic curie temperature (Tc), Blocking temperature (T_B), saturation magnetization (Ms), retentivity (Mr) coercivity (Hc) and activation energy of LCMO films are summarized.

Film	Surface Roughness (nm)	Grain diameter (nm)	Tc (K)	T_B (K)	Ms (emu/g)	Hc (Oe)	Mr (emu/g)	Ea (eV)
x = 0.0	1.86	44	150	75	721	200	455	0.21
x=0.3	2.64	46	240	179	763	410	589	0.15
x=0.5	2.27	45	245	169	288	940	199	0.16
x=0.7	2.62	51	*	48	756	20	14	0.18

* no sharp transition

The compound $La_{0.5}Ca_{0.5}MnO_3$ shows coexistence of two totally dissimilar ground states i.e. ferromagnetic-metallic and antiferromagnetic-charge ordered which is also consistent with the earlier reports [26-27]. For the doping range of x = 0.7, the compound is an antiferromagnetic insulator with the ordering of doped charge carriers. There is no sharp magnetic transition and the magnetic signal is also very low. Mathur *et al* [28] reported that when x=0.7, the crystal structure of manganite interact strongly with the corresponding magnetic and electronic structures and any imposed physical discontinuities in the actual samples will likely create or destroy the delicate phase balance.

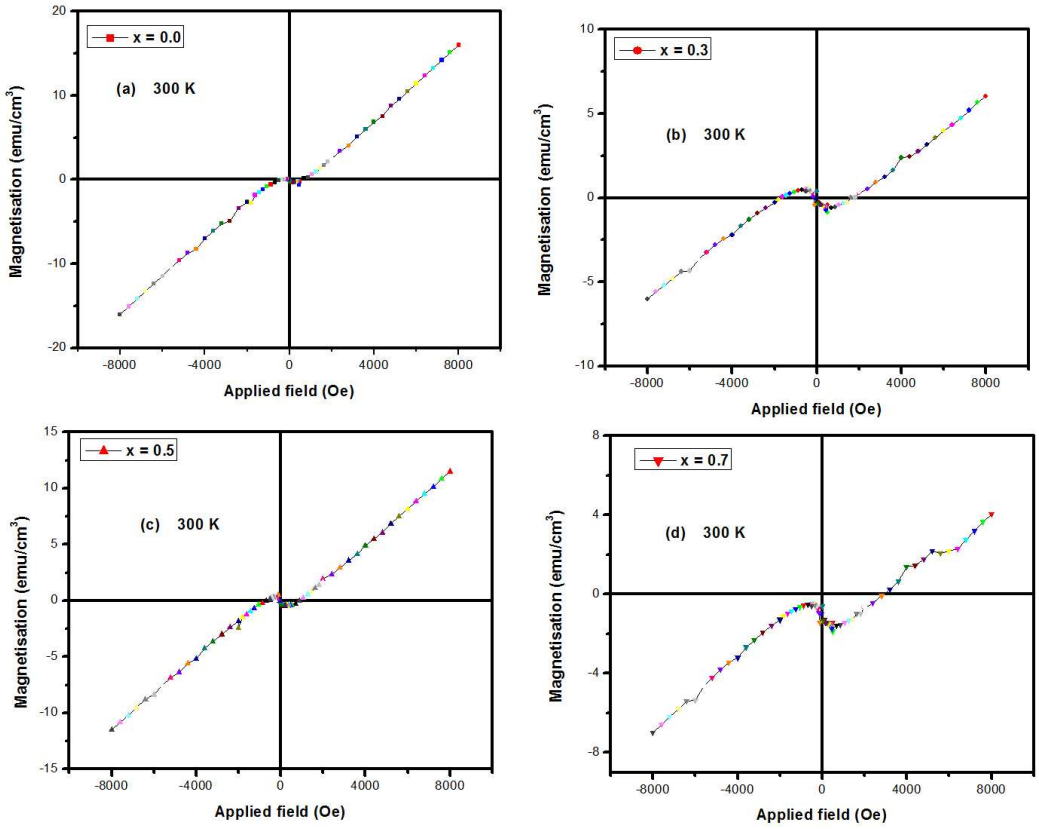

Fig.4. Magnetization vs. field curves at 300 K for LCMO thin films.

The magnetization vs. field (MH) curves at 300 K (Fig. 4) show paramagnetic behavior at room temperature and at 5 K (Fig.5 (except for the composition x = 0.7) show ferromagnetic behavior which is consistent with M vs. T data as discussed above. The magnetic hysteresis loop at room temperature (300 K) is almost paramagnetic. However below transition temperature, the films show strong ferromagnetic behavior. It is seen that the value of saturation magnetization increases up to x= 0.3 and then decreases with doping. For the composition x = 0.7, antiferromagnetic nature with the ordering of doped charge carriers. The maximum hysteresis is

observed for the composition x = 0.5. The observed large hysteresis is also reported in literature for these compounds [28-29].

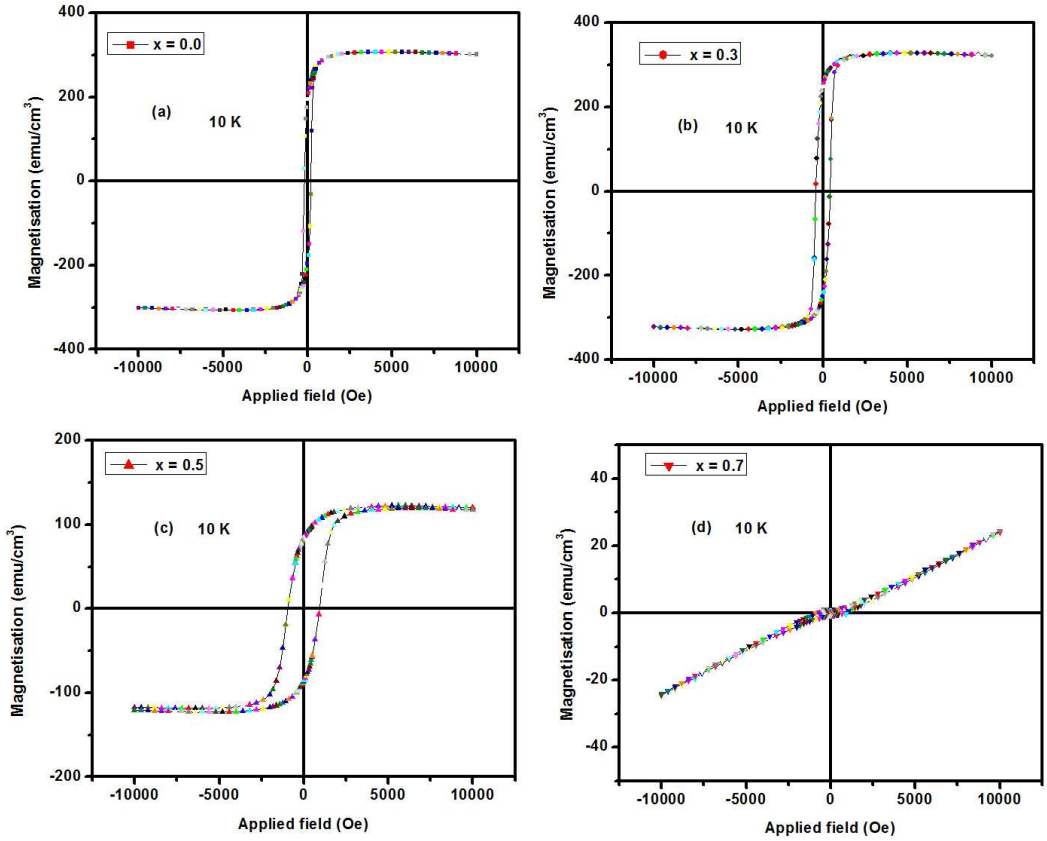

Fig.5. Magnetization vs. field curves at 10 K for LCMO films. The value of saturation magnetization increases up to x= 0.3 and then decreases with doping.

3.4. Electrical transport measurements

The electrical resistivity (ρ) of the thin films, x=0 to 0.7, both at H = 0 and H = 8 T as a function of temperature (range of 5 K-300 K) are shown in figure 6. The activation energy (E_a) was calculated from the slope of the curve log ρ vs. 1000/T (K^{-1}) using relation $\rho = \rho_0 e^{-Ea/kT}$ and the

values are tabulated in table II. Here ρ_0 is the conductivity at infinite temperature and k is the Boltzmann's constant and *Ea* is the activation energy. The pre-factor ρ_0 is of the order of 1.5 mΩ implying that the holes are localized in the paramagnetic phase. This localization is most probably due to coulomb attraction of the divalent cation or lattice distortion around it. It is clear from the table II that the value of Ea first decreases with doping but later increases for higher doping (x = 0.7). The observed trend is consistent with magnetic data in which magnetization first increase with doping for x = 0.3 and then decreases for higher doping concentrations.

All these LCMO thin films are paramagnetic insulators and have an orthorhombic crystal structure at the room temperature (300 K) [30]. There is a decrease in resistivity with Ca doping but the resistivity increases for higher doped films (x = 0.7). The data from Miller *et al.* [31] shows a sharp increase in the resistivity for both end members: $LaMnO_3$ and $CaMnO_3$. This is reminiscent of the large change in resistivity observed in semiconducting materials when donor or acceptor levels are introduced by doping with small quantities of atoms with a different valency. It is likely that the LMO film used in this investigation contains an excess of oxygen which introduces a mixed valency into the system (sometimes this process is referred to as 'self-doping') which could reduce the resistivity by an orders of magnitude. The observed trend in resistivity is in consistent with the magnetic data as well as Ea values. One of the possible explanation for the high resistivity for x = 0.7 concentration is based on the grain boundaries. It is clear from table II that the grain diameter is larger for higher doped concentration. The observed trend is also in consistent with the reports of Edwards et al [32] where they found that the grain diameter has due dependence on resistivity of the samples. In the studied polycrystalline samples, well defined grain morphology on Si substrate was observed. The zero-

field resistivity increases systematically with increasing grain size due to enhanced scattering at the grain boundaries.

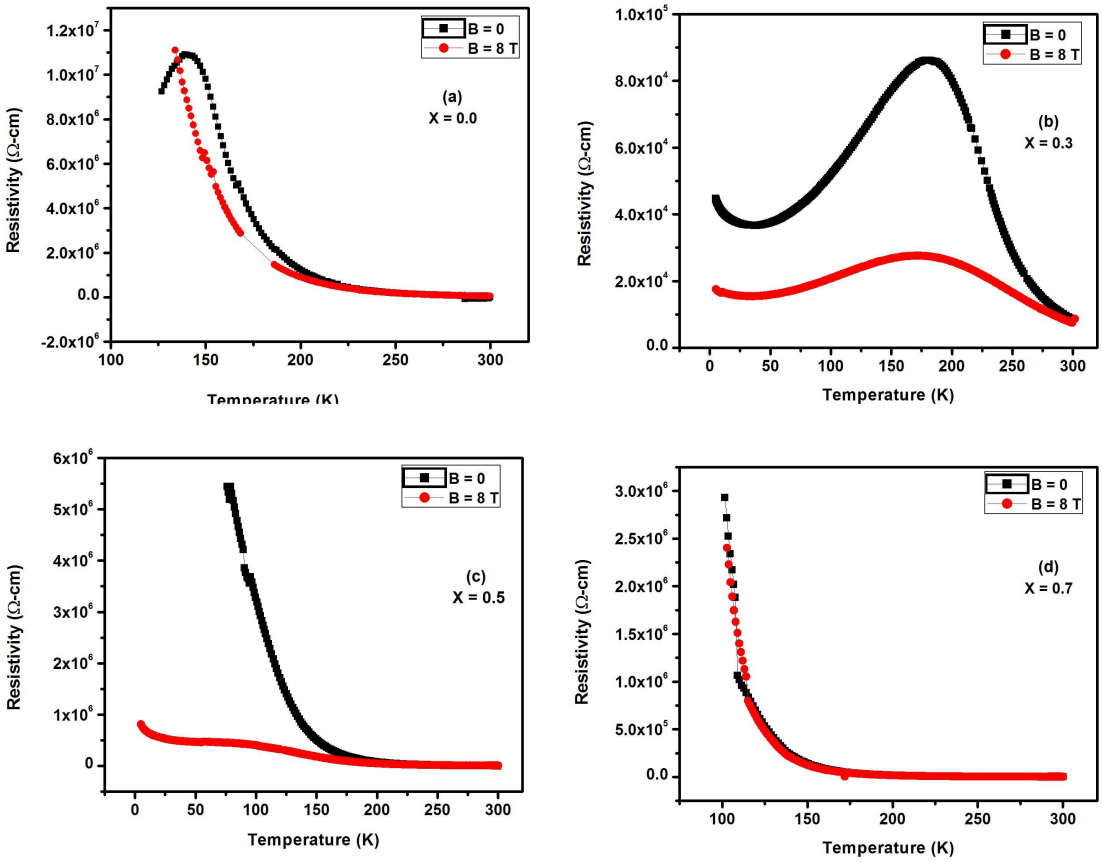

Fig.6. Temperature dependence of resistivity of LCMO films for (a) x = 0.0, (b) x = 0.3, (c) x = 0.5, (d) x = 0.7. These films show a decrease in resistivity with Ca doping but the resistivity increases for higher doped samples (x = 0.7).

The field dependent resistivity (magnetoresistance MR% = $(\rho - \rho_0 / \rho_0) \times 100$) of the films at 5 K, 100 K, 200 K and 300 K are shown in figure 7 (a)-(d) for films with (a) x= 0.0, (b) x= 0.3, (c) x= 0.5 and (d) x= 0.7.

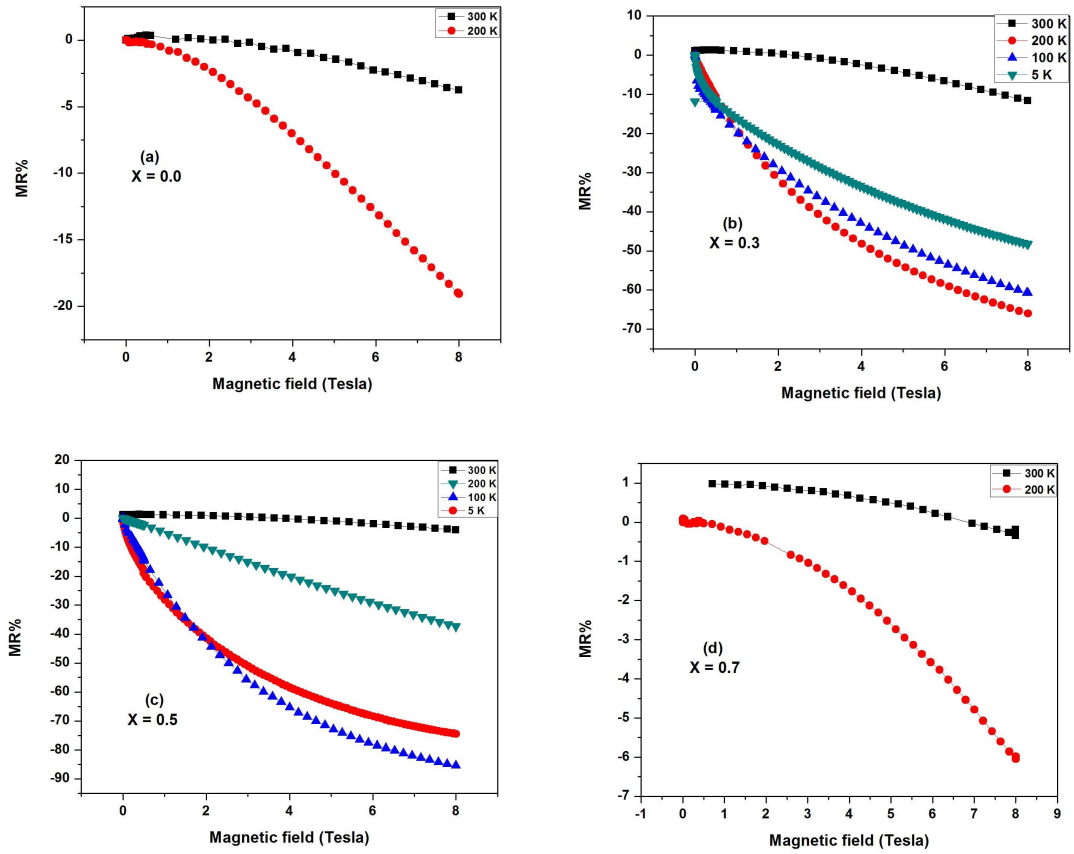

Fig.7. Magnetoresistance values of LCMO thin films for (a) x = 0.0, (b) x = 0.3, (c) x = 0.5, (d) x = 0.7. The value of MR% is max (70-80%) for intermediate doping concentrations (x = 0.3, 0.5) at H = 8 Tesla.

For x = 0.0 and x= 0.7, the MR values are only shown at 200 K and 300 K as the resistivity of these films were too high at lower temperatures. It is observed that in all doping concentrations resistivity decreases with temperature and is consistent with resistivity data as discussed above. The MR also increases with magnetic field for all doping concentrations. The value of MR% is max (70-80%) for intermediate doping concentrations (x = 0.3, 0.5) at H = 8 Tesla. There is a visible similarity in the nature of change of resistivity with Ca doping to that of dependence on magnetic Tc. Resistivity decreases sharply with Mn content reaches minimum at x=0.5 and then

increases; magnetization also increases with doping, becomes maximum at x=0.5 and then decreases. The variation of these transport properties with Ca doping reflects changes in conduction band structure which is evident from the X-ray absorption spectroscopy studies.

3.5 Electronic Structure by XAS

To understand the element specific electronic structure and chemical environment of Mn and O ions in the compound LCMO thin films, XAS studies were carried out. The normalized XAS spectra at O K edge at 300 K is shown in figure 8 (a). The electronic structure close to Fermi level (E_F) is dominated by Mn 3d and O 2p states in manganites. The O K-edge probes the unoccupied density of states with the O 2*p* symmetry due to dipole selection rules that arise mainly from the hybridization of O 2*p* states with various states of neighboring atoms, 3*d* states of Mn and also the 4*d* states of La. [33] These spectra show main features 'A', 'B', 'C' and D at 527.5, 530.6, 534.1 and 541.4 respectively. The peaks 'A' and 'B' arises from the hybridized O 2*p*-Mn 3*d* states and split into t_{2g} and e_g orbitals under the influence of octahedral crystal field [34]. The peak 'C' in fig. 8 (a) is attributed to hybridization of O 2*p* orbital with La 5*d*-states. The broad peak 'D' is attributed to the bands of higher energy metallic states, e.g. Mn 4sp and La 6sp bands. The well resolved peaks marked as 'A', 'B' in pure $LaMnO_3$ correspond to crystal field splitting energy 10 Dq ~ 2.9 eV for e_g and t_{2g} orbitals of the 3*d* energy level of Mn. All these features are commonly observed in perovskites [35] including nickelates [36], titanates [37] and manganites [38, 39].

The changes in the spectral feature of the compound LMO with the inclusion of Ca is depicted in the O K-edge difference spectra as shown in figure 8 (b). The intensity of peak B provides a measure of Mn 3*d*-state occupancy. From Fig. 8 (b) it is observed that the intensity of

peak 'B' increases with Ca-concentration. Increase in peak intensity indicates lower Mn 3*d*-state occupancy, i.e. higher Mn valency. The origin of Mn^{2+} is interpreted by suggesting a charge disproportionation model based in the instability of Mn^{3+} for the Mn^{2+} formation via $2Mn^{3+} \rightarrow Mn^{2+} + Mn^{4+}$ by Hundley et al. [33] and de Jong et al.[34]. It is also observed from the difference spectra that the density of states increases with Ca doping (see, the spectral peaks from 'A' to 'D').

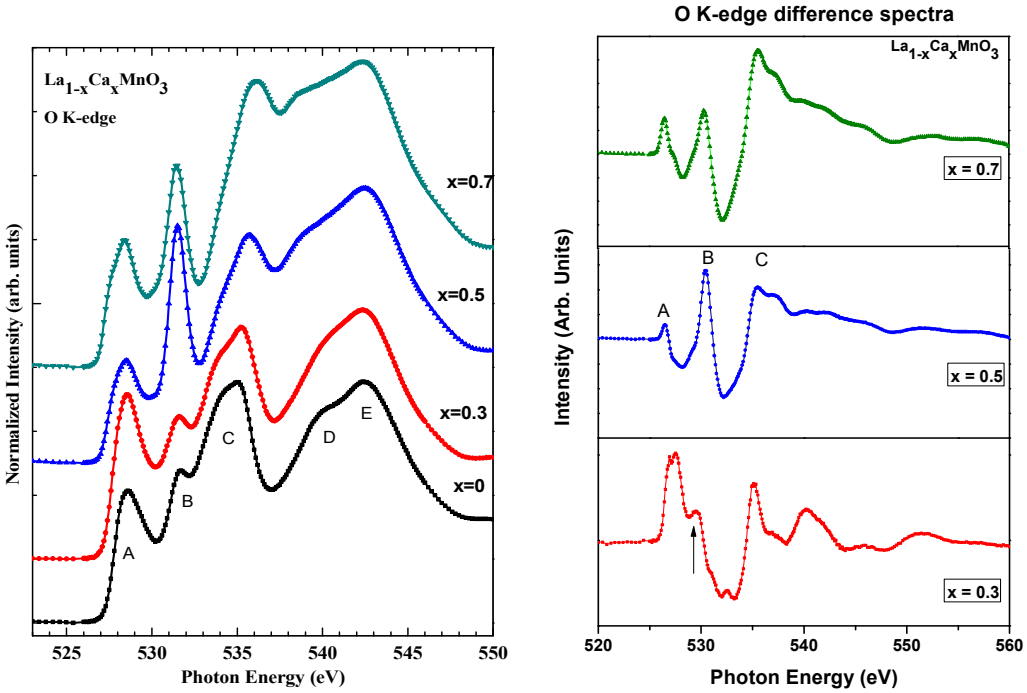

Fig.8.(a) Normalized O K-edge XAS spectra of $La_{1-x}Ca_xMnO_3$ (x=0.0, 0.3, 0.5, 0.7) thin films.**(b)** Difference spectra for same films at O K-edge. It is observed that the intensity of peak 'B' increases with Ca-concentration implying change in density of states.

Fig. 9 (a) shows XAS at Mn $L_{3,2}$–edges of LCMO films. Due to the spin-orbit splitting of the 2*p* core level, 2*p* → *d*-symmetry transitions give rise to two edges, namely $2p_{3/2}$ (L_3-edge) at 639 eV and $2p_{1/2}$ (L_2-edge) at 650 eV separated by ~11 eV. Each spectral edge has sharp peaks due to large number of conduction band 3*d*-states. Compared to $2p_{1/2}$, higher number of electrons is available in $2p_{3/2}$, because of which the intensity of the L_3-peak is expected to be higher compared to the L_2-peak. It has been reported earlier that the energy position of spectral features in Mn $L_{3,2}$ XAS study are very sensitive to the oxidation state of Mn atoms and can be used to determine the Mn valency [40-44]. The double peak feature of the L_3-edge changes as the Ca-concentration increases. The changes in the spectral feature of the compound LMO with the inclusion of Ca is depicted in the $L_{3,2}$ -edge difference spectra as shown in figure 10 (b). It is seen that the multiplet feature L_3-edge marked as 'A_1' and 'B_1'.With increase in Ca-concentration, there is change in the mixed valent states of Mn^{2+}/Mn^{3+} in the system. It is also seen that L_3-edge shifts towards higher energy and there is corresponding modification in spectral shape which is suggestive of the fact that valency of Mn changes with Ca doping [42]. It is also observed from Fig. 9 that the peak at 638.8 eV shown by 'A_1' is typical for Mn^{2+} and the peak around 640.3 eV is typical for Mn^{3+}.Therefore, if Mn is in mixed valency state, a mixture of Mn^{2+} and Mn^{3+}, it is expected to show as a double peak Mn L_3-feature. With these insights, one concludes that LCMO films contain both Mn^{2+} and Mn^{3+} ions. Due to this mixed valence state of Mn induced by the introduction of Ca in the LCMO system, multichannel double exchange mechanism (Mn^{2+}-O- Mn^{3+}, Mn^{3+}-O- Mn^{4+}) may be favored. These imply that the mixed valence state of Mn ions is responsible for modifying the magnetic and other transport properties of the LCMO system.

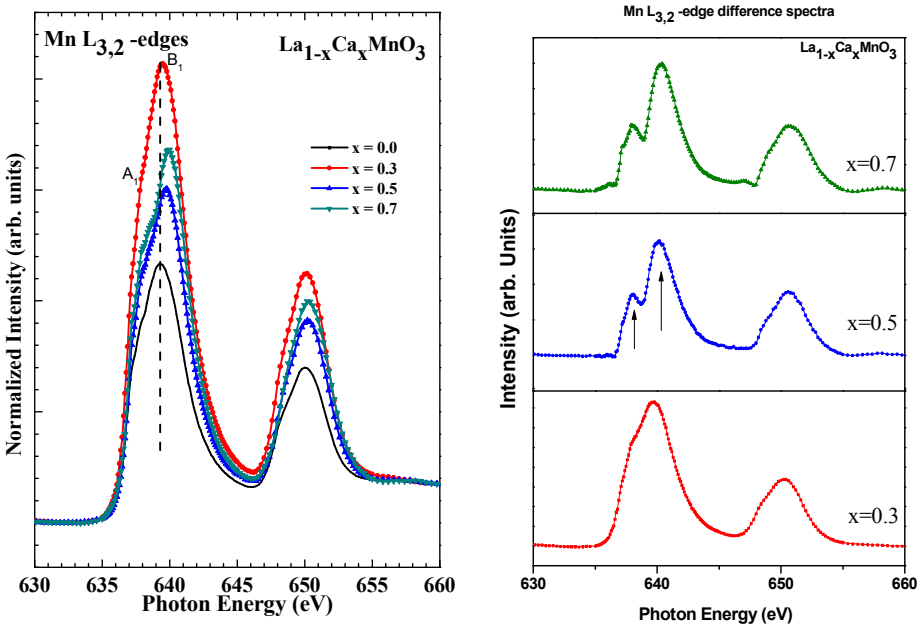

Fig.9. (a) Normalized Mn $L_{3,2}$-egde XAS spectra of LCMO thin films.**(b)** Difference spectra for Mn $L_{3,2}$-edge. Note that the Mn L_3-edge shifts towards higher energy and there is corresponding modification in spectral shape which is suggestive of the fact that valency of Mn changes with Ca doping.

The overall magnetic and electrical behavior depends on the interactions between the different Mn ions. Four counteracting processes determine the behavior of the Mn 3d valence electrons. These are: double exchange interaction, super exchange interaction, Jahn Teller effect and charge ordering. The parameters like temperature, doping, strain and crystal structure determine the dominant mechanism. Deformation of the oxygen octahedron causes energy differences within the otherwise degenerate t_{2g} and e_g electron states. While orbitals that are compressed by the deformation gain energy, the orbitals that are elongated by the deformation loose energy. When the e_g shell is half filled it is energetically favorable to create a deformation, because one of the orbitals will lose energy. The electrons in the e_g shell will then occupy this lower energy state. Creating a deformation of the oxygen octahedrons without altering the overall crystal lattice

leads to the typical Jahn Teller distortions. During double exchange interaction two neighboring Mn ions and their connecting O ion play an important role. The Mn ion in this system has one unoccupied 3d orbital. Thus, one electron from the O 2p orbital tunnels to this Mn 3d orbital. On seeing the unoccupied O 2p orbital, the electron moves from other Mn 3d orbital. The net result is one electron moving from one Mn ion to another Mn ion. The qualitative picture of this behavior in the mixed-valent manganite, $La_{0.5}Ca_{0.5}MnO_3$ has been attributed to the concept of Zener double exchange [6, 30].

The influence of substrate strain is the main factor distinguishing manganite thin films from bulk ceramic samples. $LaAlO_3$ is a commonly used substrate which has least lattice mismatch to LCMO at room temperature and hence low strain. The effect of various substrates as well as film thickness on MR has been studied by Jin *et al* [45] and observed that the strain effect, expressed through the MR is most pronounced for epitaxial films. It is speculated that stress is most effectively propagated through the film thickness in the absence of grain boundaries. For $LaAlO_3$ substrate, MR is maximized for film thickness 1000 A°. In this study, LCMO films deposited on Si (100) that has larger lattice mismatch with LCMO at room temperature (as discussed in introduction) that brings additional strain in the films. Pristine LMO is in anti-ferromagnetic insulating (AFI) state upto 150 K and then changes into paramagnetic state (PM). The x = 0.3 composition films were found to be in ferromagnetic region upto 240K, then changes into PM state. The x = 0.5 composition films were found to be in FM state upto 245K and then changes to PM state. The films with x > 0.5 (x = 0.7) films were found to be in a mixture of charge ordered insulating (COI) and AFI states. Ramirez [46] reported Tc for concentration x ~ 0.3 to be around 220 K, while in this study, it is observed it to be around 240 K. Hence the large lattice mismatch between Si and LCMO results in change in the phase

diagram of LCMO system when deposited on Si substrates. The mixed valent LCMO exhibits a large variety of states. Such variation occurs because of the presence of various competing and cooperating interactions involving the charge, orbital, spin and lattice degrees of freedom. In the present study, the interactions are described using simple ionic picture of Mn 3d orbitals. The Mn^{4+} ion contains three electrons in the t_{2g} state which are localized and have collinear spins because of the large Hund's coupling. With Ca doping in the parent compound $LaMnO_3$, the extra electron goes into the e_g orbitals. There is also a large Hund's coupling between the e_g electron and the immobile t_{2g} spin. As a result, the metallic ground state in manganites is also ferromagnetic. In the LCMO system, oxygen 2p orbitals play an essential role and are strongly hybridized with the Mn orbitals. The picture described in LCMO system can be understood as a parameterization in which the oxygen degrees of freedom are integrated, and new effective degrees of freedom are introduced by Mn 3d orbitals.

4. Conclusion

Thin films of LCMO thin films were deposited on Si (100) substrate by PLD technique and characterized by various techniques to understand their structural, morphological, electrical, magnetic properties and their electronic structures. From the magnetic measurements, it is observed that the value of Tc increases with Ca doping in the LCMO system up to x = 0.5 and there was no sharp magnetic transition at x=0.7. The value of magnetic moment increases progressively with Ca doping but decreases for higher doping (x = 0.7). The value of saturation magnetization increases up to x= 0.3 and then decreases with doping. The film with composition x = 0.7 shows an antiferromagnetic nature with the ordering of doped charge carriers. The maximum hysteresis is observed with composition x = 0.5. The MR is found to increase with

field for all doping concentrations. The value of MR% is max (70-80%) for intermediate doping concentrations (x = 0.3, 0.5) at H = 8 Tesla. Spectroscopic studies using XAS indicate increase in Mn valency confirming admixture of Mn^{2+}, Mn^{3+}, and Mn^{4+} and also suggest that the density of states increases with Ca doping. The phase diagram of Ca doped LMO exhibits significant changes with doping concentration. The pristine LMO exhibits an anti-ferromagnetic insulating (AFI) state upto 150 K and then changes into paramagnetic state (PM). As the density of states increases due to doping, at x = 0.3, LCMO films shows ferromagnetic region upto 240K, then changes into PM state. At x = 0.5, these films are found to be in FM state upto 245 K and then changes to PM state. The films with x > 0.5 (x = 0.7) films were found to be in a mixture of charge ordered insulating (COI) and AFI states. Depending upon the doping concentration different phases evolves which strongly related to their electronic structure induced by Ca dopant.

Acknowledgements

Authors (K.S and M.I) thank Dr. R.J. Choudhary, Dr. R. Rawat, Dr. V.R. Reddy IUC, CSR Indore for magnetic, transport and XRD measurements respectively and Director IUAC, New Delhi for necessary experimental facilities. They also thank the director NIT Srinagar for encouragement and support.

References

[1]. R. Korotana, G. Mallia, Z. Gercsi, L. Liborio, and N. M. Harrison, Phys. Rev. B 89, (2014) 205110.

[2]. J. A. Turcaud, A. M. Pereira, and L. F. Cohen, Phys. Rev. B **91**, (2015) 134410.

[3].C. Raisch, C. Langheinrich, R. Werner, R. Kleiner, D. Koelle, M. Glaser, T. Chassé and A. Chassé, J. Appl. Phys. **113**,(2013) 063511.

[4]. Liu Yu-Kuai, Yin Yue-Wei, and Li Xiao-Guang, Chin. Phys. B 22, (2013) 087502

[5]. A. J. Mills, Nature **392 (**1998**)** 147.

[6]. C. Zener, Phys. Rev. **81**, (1951) 440.

[7]. P. W. Anderson and H. Hasegawa, Phys. Rev. **100** (1955) 675.

[8]. P. H. de Gennes, Phys. Rev. **118** (1960) 141.

[9]. J. B. Goodenough, Annu. Rev. Mater. Sci. **28** (1998) 1.

[10]. M. Uehara, S. Mori, C. H. Chen, and S. W. Cheong, Nature, London, **399** (1999) 560.

[11]. Y. Tokura and N. Nagaosa, Science **288** (2000) 462.

[12]. A. Moreo, S. Yunoki, and E. Dagotto, Science **283** (1999) 2034.

[13]. A. Kleine, Y Luo, and K Samwer, *Euro phys. Lett.***76** (2006) **135**.

[14]. C. Aruta *et al,. J. Appl. Phys.* **100** (2006) 023910.

[15]. G. Kartopu and M. E. Souni, *J. Appl. Phys.* **99** (2006) 033501.

[16]. P. Orgaini, C. Aruta, R. Ciancio, A. Galdi and L. Maritato, *Appl. Phys. Lett.* **95** (2009)013510.

[17]. Khanduri et al. J. Phys. D: Appl. Phys. **46** (2013)175003.

[18]. H.Y. Hwang, S.W. Cheong, P.G. Radaeli, M. Marezio, B. Batlogg, Physics Review Letters 75 (1995) 914–917.

[19]. H. Dulli, P. A. Dowben, S.-H. Liou, and E. W. Plummer, Phys. Rev. B **62**, (2000) R14 629.

[20]. J. Choi, J. Zhang, S.-H. Liou, P. A. Dowben, and E. W. Plummer, Phys. Rev. B **59** (1999) 13 453.

[21]. M. V. Abrashev, J. Backstram, L. Borjesson, V.N. Popov, R. A. Chakalov , N. Kolev, R. L. Meng and M. N. Iliev, Phys. Rev. B **65** (2002) 184301.

[22]. J. Rodriguez-Carvajal, M. Hennion, F. Moussa, A. H. Moudden, L. Pinsard and A. Revcolevschi, Phys. Rev. B **57** (1998) R3189.

[23]. R. K. Zheng, C. F. Zhu, I. Q. Xie and X. G. Li, Phys. Rev. B **63** (2000) 020427.

[24]. R. V. Krishnan and A. Banerjee, DAE Solid State Phys. Symp. (India) **41** (1998) 431.

[25]. R. M. Nagabbushane, G. T. Chandrappa, R. P. Sreekanth Chakradhar and K. P. Ramesh, DAE Solid State Phys. Symp. (India) **49** (2004) 293.

[26]. A. Moreo, S. Yunoki, E. Dagotto, *Science* **283**(1999) 2034–2040.

[27]. N. D. Mathur, P. B. Littlewood, *Sol. Stat. Comm.* **119** (2001) 271-280.

[28]. M. Uehara, S. Mori, C. H. Chen, S. W. Cheong, *Nature* **399** (1999) 560–563.

[29]. P. Levy, et *al*. *Phys. Rev. B* .**62**(2000) 6437–6441.

[30]. S.W. Cheong and H.Y. Hwang in Colossal Magnetoresistive Oxides – Monographs in Condensed Matter Science. (ed. Tokura Y.), Gordon & Breach, Reading, (2000).

[31]. R. C Miller, R. R. Heikes and R. Mazelsky. *J. Appl. Phys.* **32** (1961) 3302.

[32]. P. P. Edwards, M. J. Sienko, Phys. Rev. B **17** (1978) 2575.

[33]. M. F. Hundley and J. J. Neumeier, *Phys. Rev. B* **55** (1997) 11511.

[34]. M. P. de Jong, I. Bergenti, V. A. Dediu, M. Fahlman, M. Marsi, and C. Taliani, *Phys. Rev.*

B **71** (2005) 014434.

[35] P. A van Aken, B. Liebscher and V. J Styrsa, *Phys. Chem. Minerals* **25 (**1998**)**494

[36] D. D Sarma *et al., Phys. Rev.* B **49 (**1994**)**14238.

[37] K. Asokan K *et al.,, J. Phys.: Condens. Matter* **13 (**2001**)**11087

[38] M. Abbate, D. Cruz, G. Zampieri G, J. Briatico , M. T Causa, M. Tovar , A. Caneiro , B. Alascio and E. Morikawa, *Solid State Commun.* **103 (**1997**)** 9.

[39] M. Abbate *et al., Phys. Rev.* B **46 (**1992**)**4511.

[40]. L. A. J. Garvie and A. J. Craven, *Phys. Chem. Minerals* **21** (1994) 191.

[41]. J. Kawai, Y. Mizutani, T. Sugimura, M. Sai, T. Higuchi, Y. Harada, Y. Ishiwata, A. Fukushima, M. Fujisawa, M. Watanabec, K. Maeda, S. Shin, and Y. Gohshi, *Spectr. Acta B* **55**, (2000) 1385.

[42]. S. P. Cramer, F. M. F. de Groot, Y. Ma, C. T. Chen, F. Sette, C. A. Kipke, D. M. Eichhorn, M. K. Chan, W. H. Armstrong, E. Libby, G. Christou, S. Brooker, V. McKee, O. C. Mullins, and J. C. Fuggle, *J. Am. Chem. Soc.* **113** (1991) 7937.

[43]. H. K. Schmid and W. Mader, *Micron* **37** (2006) 426.

[44]. F. M. F. de Groot, J C Fuggle, B T Thole and G A Sawatzky, Phys. Rev. **B 42** (1990)5459.

[45]. S. Jin, T. H. Tiefel, M. McCormack, H. M. O'Bryan, L. H. Chen, R. Ramesh and D. Schurig, *Appl. Phys. Lett.* **67** (1995) 557.

[46]. A. P. Ramirez, J. Phys: Condens. Matter **9** (1997) 8171 and references therein.